Nano-mechanical characterization of tension-sensitive helix bundles in talin rod

Koichiro Maki[1,2], Nobuhiko Nakao[1,2], Taiji Adachi[1,2,*]

[1] Laboratory of Biomechanics, Department of Biosystems Science, Institute for Frontier Life and Medical Sciences, Kyoto University, 53 Shogoin-Kawahara-cho, Sakyo, Kyoto 606-8507, Japan

[2] Department of Micro Engineering, Graduate School of Engineering, Kyoto University, Yoshida Honmachi, Sakyo, Kyoto 606-8501, Japan

*Corresponding author:

T. Adachi, Laboratory of Biomechanics, Department of Biosystems Science, Institute for Frontier Life and Medical Sciences, Kyoto University, 53 Shogoin-Kawahara-cho, Sakyo, Kyoto 606-8507, Japan

Tel.: +81-75-751-4853; Fax: +81-75-751-4853; E-mail: adachi@frontier.kyoto-u.ac.jp

Abstract

Tension-induced exposure of a cryptic signaling binding site is one of the most fundamental mechanisms in molecular mechanotransduction. Helix bundles in rod domains of talin, a tension-sensing protein at focal adhesions, unfurl under tension to expose cryptic vinculin binding sites. Although the difference in their mechanical stabilities would determine which helix bundle is tension-sensitive, their respective mechanical behaviors under tension have not been characterized. In this study, we evaluated the mechanical behaviors of residues 486–654 and 754–889 of talin, which form helix bundles with low and high tension-sensitivity, by employing AFM nano-tensile testing. As a result, residues 754–889 exhibited lower unfolding energy for complete unfolding than residues 486–654. In addition, we found that residues 754–889 transition into intermediate conformations under lower tension than residues 486–654. Furthermore, residues 754–889 showed shorter persistence length in the intermediate conformation than residues 486–654, suggesting that residues 754–889 under tension exhibit separated α-helices, while residues 486–654 assume a compact conformation with inter-helix interactions. Therefore, we suggest that residues 754–889 of talin work as a tension-sensitive domain to recruit vinculin at the early stage of focal adhesion development, while residues 486–654 contribute to rather robust tension-sensitivity by

recruiting vinculin under high tension.

Keywords

Talin; Atomic force microscopy (AFM); Nano-tensile testing; Mechanotransduction; Vinculin; Helix bundle

Highlights

- Nano-mechanical behaviors of tension-sensitive helix bundles in talin were tested.
- Residues 754-889 formed less stable helix bundle than that of residues 486-654.
- Residues 754-889 transited intermediate conformations under low tension.
- Residues 754-889 showed smaller tensile stiffness than that of residues 486-654.

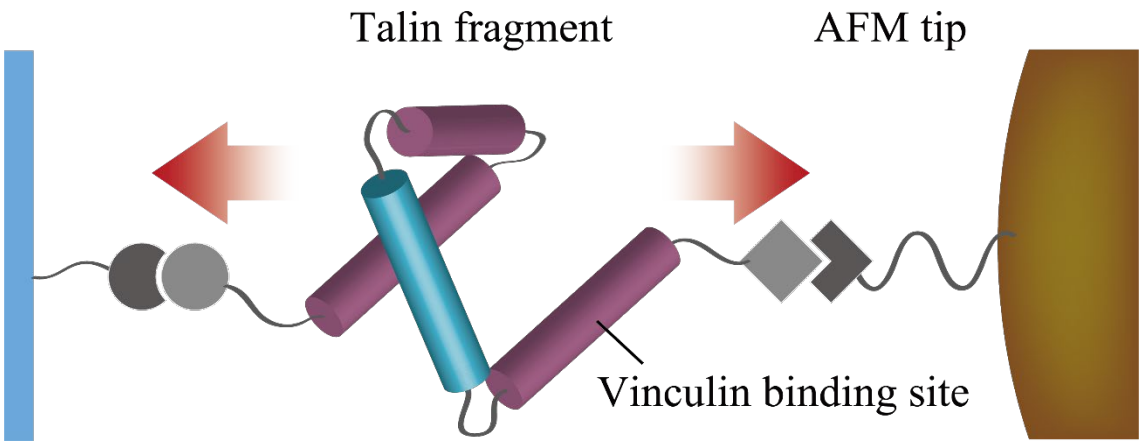

Introduction

Focal adhesion-mediated physical connection between the intercellular actin cytoskeleton and the extracellular matrix (ECM) is crucial in a variety of cellular processes such as cell growth, motility, and differentiation [1–4]. The architecture of focal adhesions exhibits sophisticated molecular layers of integrin, paxillin, talin, vinculin, zyxin, VASP, α-actinin, and so on [5]. As the size of focal adhesions corresponds to intercellular tension [6], focal adhesions are endowed with a feedback system to remodel their molecular architecture by reacting to intercellular tension. The tension-induced architectural remodeling is modulated by the tension-sensitivity of talin to recruit vinculin [7–10], which associates with actin filament [11]. The tension-sensing domain, called as a rod domain, forms helix bundles in series, some of which contain cryptic vinculin binding sites (VBSs) [12–14]. VBS-containing helix bundles unfurl under tension to expose the VBSs [15–18]. Thereby, their mechanical stabilities would be critical for determining which helix bundle is sensitive or insensitive to tension. According to the previous study [19], N-terminal helix bundles in a talin rod (residues 482–911) form a particularly tension-sensitive region. Furthermore, the tension sensitivities of the N-terminal helix bundles are known to vary according to their thermal instabilities [20]; thermally instable residues 754–889 exhibit higher

tension-sensitivity than residues 486–654. However, little is known about the nano-mechanical behaviors of tension-sensitive helix bundles under tension that direct the tension-sensitivity.

Nano-tensile testing, or single-molecule force spectroscopy, is a powerful tool for investigating the forces and motions associated with biological molecules and enzymatic activities [21,22]. In nano-tensile testing using atomic force microscopy (AFM), biomolecules modified on the substrate are directly tested by the AFM tip. The force F versus extension ΔL curves obtained in the testing contain a lot of valuable information about the mechanical behaviors of biomolecules under tension, such as their mechanical stabilities, unfolding pathways with multiple intermediate states, and mechanical properties as a polymer chain [23–26]. This technique is thus occasionally described as “mechanical fingerprinting” [27]. AFM nano-tensile testing has been utilized to explore the mechanical behaviors of α-catenin [28], a tension-sensor at adherens junctions recruiting vinculin under tension, similarly to talin.

In this study, we employed AFM-based nano-tensile testing to characterize the nano-mechanical behaviors of residues 486–654 and 754–889 of talin, which form helix bundles with low and high tension-sensitivities. Based on the force curves obtained in nano-tensile testing, we evaluated 1) the unfolding energy for the complete unfolding of

talin molecules, 2) the unfolding force required to transition to intermediate conformations, and 3) the persistence length, which describes the flexibility of intermediate conformations as a worm-like chain (WLC) polymer.

Materials and Methods

Protein purification

In this experiment, we examined residues 486-654 and 754-889 of talin. The tension-sensitive rod domain of talin, as shown in Fig. 1a, consists of serially connected helix bundles (purple, cyan, and green boxes). Some of the helix bundles contain cryptic VBSs (magenta ellipses) inside their tertiary structures. The three dimensional structure of helix bundles formed by residues 486-654 and 754-889 are shown in Fig. 1b [13,14]. DNA fragments of human talin (residues 486–654 and 754–889) were amplified by PCR and cloned into the pGEX6P-3 vector (GE Healthcare). The plasmids were verified by DNA sequencing and transformed into *Escherichia coli* strain BL21Star (DE3) cells (Invitrogen). BL21Star cells, expressing talin molecules at 20°C in Luria–Bertani medium with 0.1 mM isopropyl-β-D-thiogalactopyranoside, were suspended in 20 mM Tris-HCl buffer (pH 8.0) containing 150 mM NaCl and disrupted by sonication. After ultracentrifugation, the supernatant was applied to a Glutathione Sepharose 4B

column (GE Healthcare) to allow the binding between glutathione and GST-tag at the N-terminus of talin molecules. Eluted proteins were further purified by anion exchange (HiTrap Q HP, GE Healthcare) and then gel filtration chromatography (Superdex 200 pg, GE Healthcare).

Chemical modification for glass substrates and AFM tips

For nano-tensile testing using AFM, glass substrates and AFM tips were treated in a chemical modification process, as illustrated in Fig. 1c. The glass substrates were modified with talin at its C-terminus and the AFM tips were modified with glutathione, which associates with the GST-tag of talin at its N-terminus. The glass substrates were cleaned in a plasma cleaner and treated for 15 min with 2% MPTMS/ethanol, a silanization agent, to introduce thiol groups into the glass surface. The substrates were then treated with 2 mM maleimide-C3-NTA (Mal-C3-NTA; DOJINDO Lab.)/PBS for 30 min, with 10 mM $NiCl_2$ (Wako Pure Chemical Industries)/Milli-Q for 30 min, and washed with PBS. Talin fragments (100 μM for each fragment) were modified by NTA-Ni^{2+}-His_6 binding for 1 h and finally washed with working buffer (10 mM HEPES, 150 mM NaCl, pH 7.2). Silicon nitride AFM tips (OMCL-TR400PSA-1; spring constant, 0.02 N/m, Olympus Co.) were first cleaned in a plasma cleaner and treated for 15 min

with 2% APTES/ethanol, a silanization agent, to introduce amine groups into the glass surface. The AFM tips were then treated with 1.5 mM Mal-PEG-NHS ester/PBS for 30 min and with 10 mM glutathione/PBS for 1 h. The remaining maleimide was quenched with 50 mM 2-mercaptoethanol/HEPES and finally washed with working buffer.

AFM nano-tensile testing

For nano-tensile testing using AFM, we approached the talin-modified glass substrate with the glutathione-modified AFM cantilever and retracted the cantilever to load talin molecules directly. For this approach, we set a sampling grid on the substrate with an interval of > 100 nm, so that every molecule was tested at only one time. The piezo moving speed was kept constant at 500 nm/s. As a result, we obtained force curves, which described the mechanical behaviors of residues 486–654 and 754–889 of talin.

Force curve analysis

To analyze the complete unfolding behaviors of single talin fragments, we first extracted the force curves based on the thresholds of force at the final force peak at the rupture event, by assuming an 85%-extended WLC model [29],

$$F(\Delta L) = \frac{k_B T}{l_{pf}} \left[\frac{1}{4} \left(1 - \frac{\Delta L}{L_f} \right)^{-2} + \frac{\Delta L}{L_f} - \frac{1}{4} \right], \quad (1)$$

where k_B is the Boltzmann constant, T is temperature [300 K], and l_{pf} is the final persistence length [0.4 nm]. The fully extended length L_f was estimated as 67.2 nm (residues 486–654) and 54.0 nm (residues 754–889) based on the number of residues. For the extracted force curves, we determined PEG length L_{PEG}, which causes an additional extension in the force curves, by fitting the WLC model considering PEG length L_{PEG} as:

$$F(\Delta L) = \frac{k_B T}{l_{pf}} \left[\frac{1}{4} \left(1 - \frac{\Delta L}{L_f + L_{PEG}} \right)^{-2} + \frac{\Delta L}{L_f + L_{PEG}} - \frac{1}{4} \right], \quad (2)$$

to the final force peak. To predict the intermediate conformations of talin fragments under tension, we analyzed the persistence length l_p in the intermediate states, by fitting the WLC model with the determined L_{PEG} as:

$$F(\Delta L) = \frac{k_B T}{l_p} \left[\frac{1}{4} \left(1 - \frac{\Delta L}{L + L_{PEG}} \right)^{-2} + \frac{\Delta L}{L + L_{PEG}} - \frac{1}{4} \right], \quad (3)$$

to each force peak except the final peak, where L is the contour length of intermediate conformations.

Results

Force curves of residues 486–654 and 754–889 of talin

As a result of nano-tensile testing, we obtained force curves, as shown in Figs. 2a (residues 486–654) and 2b (residues 754–889). The possibility of complete unfolding

1 was 4.53% (376 events in 8297 trials) for residues 486–654 and 3.11% for residues
2 754–889 (464 events in 14,903 trials). The force curves are shown shifted left with the
3 PEG length L_{PEG} estimated for each curve, as illustrated in Fig. 2c. The force curves in
4 Figs. 2a and 2b show multiple force peaks caused by conformational transitions before
5 the final peak, as depicted in Fig. 2c. To reveal the mechanical behaviors of residues
6 486–654 and 754–889 of talin under tension, we measured (i) unfolding energy E_u (gray
7 area in the left panel), which is the total energy required for the complete unfolding of
8 talin, (ii) unfolding force F_u (green arrow in the right panel), which is the peak force
9 required for each conformational transition, and (iii) persistence length l_p as a WLC
10 polymer (orange dotted line in the right panel), which describes the bending stiffness
11 and apparent tensile stiffness of the intermediate conformations.
12
13 **Unfolding energy E_u required for complete unfolding of talin**
14 The histogram of the unfolding energy E_u for residues 486–654 of talin showed a
15 distribution with a peak at 2500 kJ/mol to 3500 kJ/mol, as shown in Fig. 3a (purple
16 bars). In contrast, the histogram for residues 754–889 of talin (cyan bars) showed a
17 rather right-skewed distribution, with a peak at 1500 kJ/mol to 2000 kJ/mol, which was
18 smaller than that for residues 486–654 of talin. The median value of E_u for residues

754–889 of talin was significantly larger than that for residues 486–654, as examined by the Mann-Whitney *U* test ($p < 0.001$). This indicated that residues 754–889 of talin completely unfold more easily than residues 486–654 under tension. We suggest that this difference in the unfolding energy E_u between residues 486–654 and 754–889 of talin was not just caused by the difference in the number of α-helices in each helix bundle (five α-helices in residues 486–654 and four α-helices in residues 754–889, as shown in Fig. 1b), as residues 276–393 of α-catenin, forming a four-helix bundle, showed a high unfolding energy E_u of ~3000 kJ/mol in a previous study [28]. Therefore, we suggest that the helix bundle of residues 754–889 exhibits remarkably lower mechanical stability than that of residues 486–654.

Conformational transitions of talin under tension

To compare the tendency of conformational transitions between residues 486–654 and 754–889 under tension, we analyzed the unfolding force F_u at force peaks, as described in Fig. 2c (right panel). As shown in Fig. 3b, residues 486–654 of talin showed greater unfolding force F_u of 200.4 ± 92.8 (mean ± S.D.) pN than residues 754–889 (162.3 ± 89.9 pN). Residues 754–889 showed force peaks with small unfolding force F_u (< 100 pN) with more probability density than residues 486–654. Interestingly, the average

number of force peaks with small unfolding force F_u (< 100 pN) was 1.22 peaks/curve for residues 754–889, which was twice that for residues 486–654 (0.63 peaks/curve). These results indicated that residues 754–889 transition to a larger number of intermediate conformations under low tension than residues 486–654.

Tension-induced intermediate conformations of talin as a polymer chain

To explore the intermediate conformations of residues 486–654 and 754–889 of talin, we analyzed the persistence length l_p in the force peaks assuming a WLC polymer, as explained in Fig. 2c (orange curves in the right panel). As shown in Fig. 3c, the persistence length l_p of residues 754–889, 0.19 ± 0.15 (mean ± S.D.) nm, was significantly longer than that of residues 486–654 (0.11 ± 0.08 nm), as examined by *t*-test ($p < 0.001$). As the intramolecular interactions decrease the persistence length l_p of proteins [30,31] , it was suggested that residues 486–654 under tension exhibit compact intermediate states with intramolecular interactions such as hydrophobic interactions between amphipathic α-helices, as illustrated in Fig. 3d (top panel). In contrast, residues 754–889 would exhibit more separated α-helices with more VBSs exposed to solvent (bottom panel). Since the longer persistence length l_p correlates with the smaller apparent tensile stiffness k_u, our results implied that residues 754–889 exhibit lower

apparent tensile stiffness k_u in their intermediate conformation than residues 486–654 (Fig. 3e). Thus, the small tensile stiffness k_u and small unfolding force F_u of residues 754–889 are consistent with the small unfolding energy E_u.

Discussion

In our study, we examined the mechanical behaviors of residues 486–654 and 754–889 of talin under tension by employing AFM nano-tensile testing. Residues 754–889 of talin are known to form a thermally unstable helix bundle compared with residues 486–654 [20], although their mechanical behaviors under tension have remained unclear. Our data suggested that, under tension, residues 754–889 of talin are easier to unfold with smaller unfolding energy E_u than residues 486–654, as shown in Fig. 3a. This result is consistent with the analysis of the unfolding force F_u, in which we revealed that residues 754–889 transition to intermediate conformations under lower tension than residues 486–654 do, as depicted in Fig. 3b. In addition, based on the analysis of persistence length l_p, we suggested that residues 754–889 exhibit more separated α-helices with more exposed VBSs in their intermediate conformation than residues 486–654, as illustrated in Fig. 3d. Such a difference in tension-induced intermediate conformations of VBS-containing helix bundles in talin is consistent with the results of

molecular dynamics (MD) simulation [32]. Thus, we suggest that residues 754–889 of talin work as a tension-sensitive domain to recruit vinculin in the early developmental stage of focal adhesion, while residues 486–654 contribute to rather robust tension-sensation recruiting vinculin under high tension.

The unfolding energy E_u in our experiment was estimated to be 10–100 times greater than that for other helix bundle proteins examined by thermal methods, such as differential scanning calorimetry [33,34]. We consider that the high loading rate of 10,000 pN/s adopted in this study would cause high unfolding energy E_u because the unfolding force F_u at each force peak increases with increased loading rate according to the Bell-Evans model [35,36]. To elucidate the unfolding energy E_u with a minimal effect of loading rate, another type of loading method such as "force-clamp," in which applied force is kept constant during the measurement, would be helpful. Nevertheless, our experimental method with a high loading rate has a great advantage for observing an infinitesimal conformational transition as a force peak with magnified force drop ΔF. Therefore, we suggest that both of the approaches of constant speed and constant force need to be utilized to explore intricate conformational transitions in proteins induced by force.

The conformation of unstable residues 754–889 could change due to the

interaction with the neighboring α-helices. Although the 9th to 12th α-helices of talin rod in residues 754–889 form a helix bundle, the 10th to 13th α-helices in residues 787–911 are also known to form another type of helix bundle [19]. Nevertheless, the helix bundle formed by residues 787-911 is also suggested to be less stable than that of 486-654 residues [37]. Furthermore, it is suggested that the 9th to 12th α-helices in residues 754–889 could form a seven-helix bundle together with the 6th to 8th α-helices [14]. Such various forms of VBS-containing helix bundles imply that the tension-sensitivities of VBS-containing helix bundles could dynamically change upon interaction with other α-helices.

The molecular conformations of talin *in vivo* need to be discussed further. By employing iPALM-based 3D super-resolution microscopy, Kanchanawong *et al.* (2010) revealed that talin molecules at focal adhesions in HUVEC cells are extended with an end-to-end distance of ~25 nm. However, if we consider that all of the helix bundles in talin rod domains unfurl into separated α-helices, the end-to-end distance is estimated as ~120 nm because the rod domain consists of 62 α-helices and the end-to-end distance of each α-helix is ~2 nm. This estimation implies that a couple of mechanically unstable helix bundles, such as residues 754–889, preferentially unfurl with a long end-to-end distance of ~10 nm, while other mechanically stable helix bundles, such as residues

486–654, remain folded with a short end-to-end distance. The stable helix bundles could further unfurl when focal adhesions are subjected to higher tension in particular cell activities, such as migration. Therefore, we suggest that the variation in mechanical stability of helix bundles enables talin to serve as a multi-step tension-sensor at focal adhesions.

Acknowledgements

We thank Toshio Hakoshima and Yoshinori Hirano for giving us the talin fragments. This work was partly supported by CREST from JST, Japan, and by the Grant-in-Aid for Challenging Exploratory Research (15K13832) from the JSPS, Japan. Koichiro Maki was supported by the JSPS Research Fellowships for Young Scientists.

Conflict of interest

The authors declare no competing financial interests.

References

[1] R.O. Hynes, Extracellular matrix: not just prety fibrils, Science. 326 (2009) 1216–1219.

[2] D.B. Wormer, K.A. Davis, J.H. Henderson, C.E. Turner, The focal adhesion-localized CdGAP regulates matrix rigidity sensing and durotaxis, PLoS One. 9 (2014) e91815.

[3] A.J. Engler, S. Sen, H.L. Sweeney, D.E. Discher, Matrix elasticity directs stem cell lineage specification, Cell. 126 (2006) 677–689.

[4] J.C. Kuo, Mechanotransduction at focal adhesions: integrating cytoskeletal mechanics in migrating cells, J. Cell. Mol. Med. 17 (2013) 704–712.

[5] P. Kanchanawong, G. Shtengel, A.M. Pasapera, E.B. Ramko, M.W. Davidson, H.F. Hess, C.M. Waterman, Nanoscale architecture of integrin-based cell adhesions, Nature. 468 (2010) 580–584.

[6] J.M. Goffin, P. Pittet, G. Csucs, J.W. Lussi, J.J. Meister, B. Hinz, Focal adhesion size controls tension-dependent recruitment of α-smooth muscle actin to stress fibers, J. Cell Biol. 172 (2006) 259–268.

[7] F. Margadant, L.L. Chew, X. Hu, H. Yu, N. Bate, X. Zhang, M. Sheetz, Mechanotransduction in vivo by repeated talin stretch-relaxation events depends

upon vinculin, PLoS Biol. 9 (2011) e1001223.

[8] W.H. Ziegler, A.R. Gingras, D.R. Critchley, J. Emsley, Integrin connections to the cytoskeleton through talin and vinculin, Biochem. Soc. Trans. 36 (2008) 235–239.

[9] J. Liu, Y. Wang, W.I. Goh, H. Goh, M.A. Baird, S. Ruehland, S. Teo, N. Bate, D.R. Critchley, M.W. Davidson, P. Kanchanawong, Talin determines the nanoscale architecture of focal adhesions, Proc. Natl. Acad. Sci. U. S. A. 112 (2015) 4864–4873.

[10] H. Hirata, H. Tatsumi, C.T. Lim, M. Sokabe, Force-dependent vinculin binding to talin in live cells: a crucial step in anchoring the actin cytoskeleton to focal adhesions, Am. J. Physiol. Cell Physiol. 306 (2014) 607–620.

[11] C. Grashoff, B.D. Hoffman, M.D. Brenner, R. Zhou, M. Parsons, M.T. Yang, M.A. McLean, S.G. Sligar, C.S. Chen, T. Ha, M.A. Schwartz, Measuring mechanical tension across vinculin reveals regulation of focal adhesion dynamics, Nature. 466 (2010) 263–266.

[12] G.C.K. Roberts, D.R. Critchley, Structural and biophysical properties of the integrin-associated cytoskeletal protein talin, Biophys. Rev. 1 (2009) 61–69.

[13] E. Papagrigoriou, A.R. Gingras, I.L. Barsukov, N. Bate, I.J. Fillingham, B. Patel,

R. Frank, W.H. Ziegler, G.C.K. Roberts, D.R. Critchley, J. Emsley, Activation of a vinculin-binding site in the talin rod involves rearrangement of a five-helix bundle, EMBO J. 23 (2004) 2942–2951.

[14] I. Fillingham, A.R. Gingras, E. Papagrigoriou, B. Patel, J. Emsley, D.R. Critchley, G.C.K. Roberts, I.L. Barsukov, A vinculin binding domain from the talin rod unfolds to form a complex with the vinculin head, Structure. 13 (2005) 65–74.

[15] T. Izard, C. Vonrhein, Structural basis for amplifying vinculin activation by talin, J. Biol. Chem. 279 (2004) 27667–27678.

[16] S.E. Lee, R.D. Kamm, M.R.K. Mofrad, Force-induced activation of talin and its possible role in focal adhesion mechanotransduction, J. Biomech. 40 (2007) 2096–2106.

[17] J. Golji, M.R.K. Mofrad, A molecular dynamics investigation of vinculin activation, Biophys. J. 99 (2010) 1073–1081.

[18] V.P. Hytönen, V. Vogel, How force might activate talin's vinculin binding sites: SMD reveals a structural mechanism, PLoS Comput. Biol. 4 (2008) e24.

[19] B.T. Goult, T. Zacharchenko, N. Bate, R. Tsang, F. Hey, A.R. Gingras, P.R. Elliott, G.C.K. Roberts, C. Ballestrem, D.R. Critchley, I.L. Barsukov, RIAM and

vinculin binding to talin are mutually exclusive and regulate adhesion assembly and turnover, J. Biol. Chem. 288 (2013) 8238–8249.

[20] B. Patel, A.R. Gingras, A.A. Bobkov, L.M. Fujimoto, M. Zhang, R.C. Liddington, D. Mazzeo, J. Emsley, G.C.K. Roberts, I.L. Barsukov, D.R. Critchley, The activity of the vinculin binding sites in talin is influenced by the stability of the helical bundles that make up the talin rod, J. Biol. Chem. 281 (2006) 7458–7467.

[21] X. Zhuang, M. Rief, Single-molecule folding, Curr. Opin. Struct. Biol. 13 (2003) 88–97.

[22] C.T. Lim, E.H. Zhou, A. Li, S.R.K. Vedula, H.X. Fu, Experimental techniques for single cell and single molecule biomechanics, Mater. Sci. Eng. C. 26 (2006) 1278–1288.

[23] H. Janovjak, M. Kessler, D. Oesterhelt, H. Gaub, D.J. Müller, Unfolding pathways of native bacteriorhodopsin depend on temperature, EMBO J. 22 (2003) 5220–5229.

[24] I. Popa, P. Kosuri, J. Alegre-Cebollada, S. Garcia-Manyes, J.M. Fernandez, Force dependency of biochemical reactions measured by single-molecule force-clamp spectroscopy, Nat. Protoc. 8 (2013) 1261–1276.

[25] M. Rief, M. Gautel, F. Oesterhelt, J.M. Fernandez, H.E. Gaub, Reversible unfolgind of individual titin immunoglobulin domains by AFM, Science. 276 (1997) 1109–1112.

[26] K. Maki, S.W. Han, T. Adachi, β-Catenin as a tension transmitter revealed by AFM nanomechanical testing, Cell. Mol. Bioeng. 8 (2015) 14–21.

[27] T. Hoffmann, L. Dougan, Single molecule force spectroscopy using polyproteins, Chem. Soc. Rev. 41 (2012) 4781–4796.

[28] K. Maki, S.W. Han, Y. Hirano, S. Yonemura, T. Hakoshima, T. Adachi, Mechano-adaptive sensory mechanism of α-catenin under tension, Sci. Rep. 6 (2016) 24878.

[29] C. Bustamante, J.F. Marko, E.D. Siggia, S. Smith, Entropic elasticity of λ-phage DNA, Science. 265 (1994) 1599–1600.

[30] K.A. Walther, F. Gräter, L. Dougan, C.L. Badilla, B.J. Berne, J.M. Fernandez, Signatures of hydrophobic collapse in extended proteins captured with force spectroscopy, Proc. Natl. Acad. Sci. U. S. A. 104 (2007) 7916–7921.

[31] G. Stirnemann, D. Giganti, J.M. Fernandez, B.J. Berne, Elasticity, structure, and relaxation of extended proteins under force, Proc. Natl. Acad. Sci. U. S. A. 110 (2013) 3847–3852.

[32] A.W.M. Haining, M. Von Essen, S.J. Attwood, V.P. Hytönen, A. Del Río Hernández, All subdomains of the talin rod are mechanically vulnerable and may contribute to cellular mechanosensing, ACS Nano. 10 (2016) 6648–6658.

[33] P. Huang, G. Oberdorfer, C. Xu, X.Y. Pei, B.L. Nannenga, J.M. Rogers, F. Dimaio, T. Gonen, B. Luisi, D. Baker, High thermodynamic stability of parametrically designed helical bundles, Science. 346 (2014) 481–485.

[34] M. Munson, R. O'Brien, J.M. Sturtevant, L. Regan, Redesigning the hydrophobic core of a four-helix-bundle protein, Protein Sci. 3 (1994) 2015–2022.

[35] G.I. Bell, Models for the specific adhesion of cells to cells, Science. 200 (1978) 618–627.

[36] E. Evans, K. Ritchie, Strength of a weak bond connecting flexible polymer chains, Biophys. J. 76 (1999) 2439–2447.

[37] M. Yao, B.T. Goult, H. Chen, P. Cong, M.P. Sheetz, J. Yan, Mechanical activation of vinculin binding to talin locks talin in an unfolded conformation, Sci. Rep. 4 (2014) 4610.

Figures

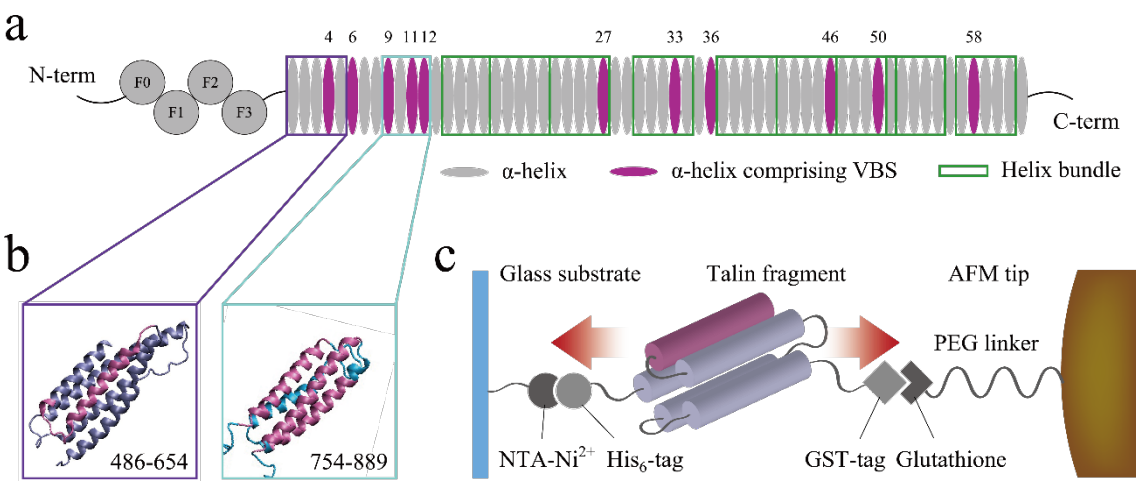

Fig. 1 Nano-tensile testing of helix bundles in talin rod employing AFM.

(a) The structural domains of talin. The tension sensitivity of talin is modulated by a central rod domain, which consists of 62 α-helices (gray and magenta ellipses). Most vinculin binding sites (VBSs; magenta ellipses) are embedded in helix bundles (purple, cyan and green boxes), which are formed by four or five amphipathic α-helices based on hydrophobic interaction. **(b)** Crystal structures of residues 486–654 (left panel, PDB code: 1SJ7) and 754–889 (right panel, PDB code: 1U89) of talin. In both panels, VBSs are shown in magenta. **(c)** Schematics of nano-tensile testing employing AFM. Single talin molecules, which were chemically modified on the glass substrate by His_6-Ni^{2+}-NTA affinity, were captured by the AFM tip using GST-glutathione affinity and directly loaded.

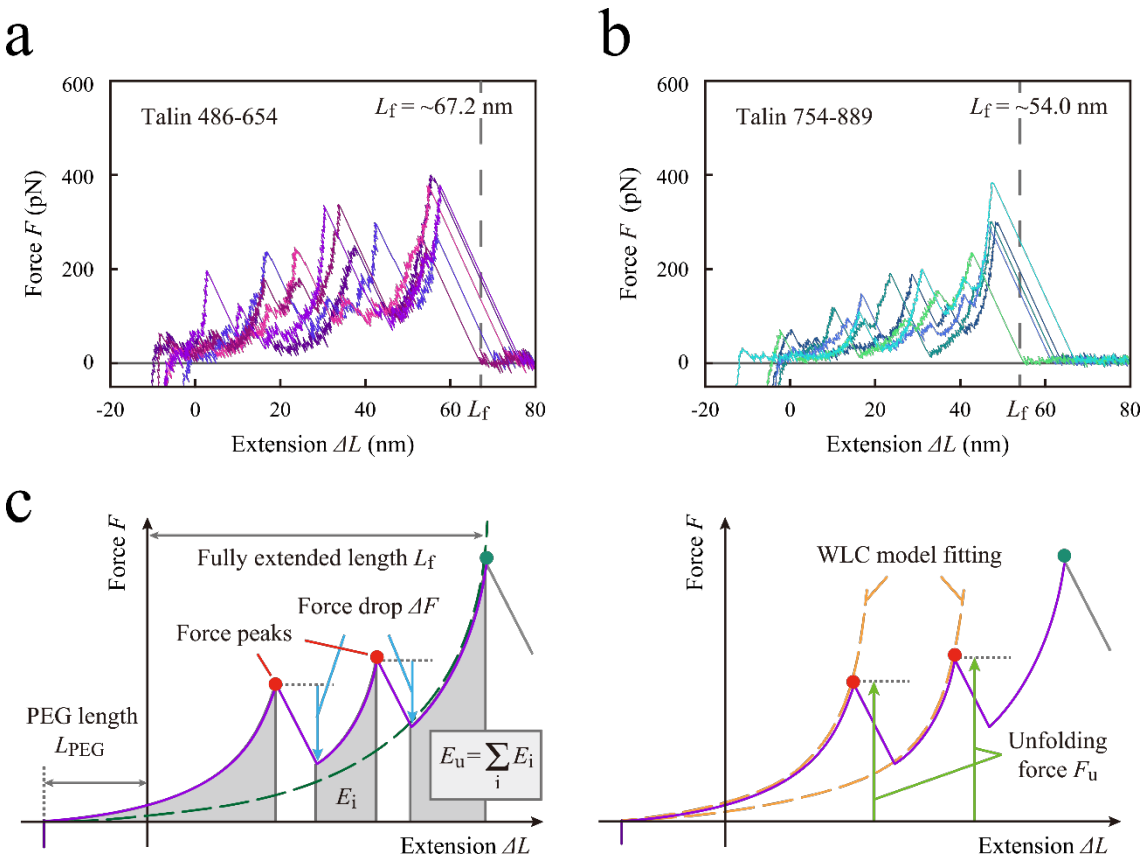

Fig. 2 Force curves for residues 486–654 and 754–889 of talin.

(a, b) Force curves obtained for residues 486–654 and 754–889. Five typical force curves are superimposed and shown in each panel. The force curves are shifted left by the estimated PEG length L_{PEG}, which causes an additional extension in the force curves. The vertical dashed lines indicate the fully extended length L_f of each fragment (67.2 nm for residues 486–654 and 54.0 nm for residues 754–889, estimated based on the number of residues). **(c)** Analytical methods for force curves (purple lines). The PEG length L_{PEG} was estimated by the WLC fitting to the final peak (green dashed line). As shown in the left panel, force peaks (red dots) except the final peak (green dot) were

identified with the following force drop ΔF on the basis of the threshold (20 pN). We first evaluated the unfolding energy E_u by summing all of the intermediate unfolding energy E_i (gray area). As shown in the right panel, the unfolding force F_u (green line) was calculated for each force peak. The persistence length l_p of intermediate conformations was evaluated by fitting to a WLC model (orange dashed line, right panel).

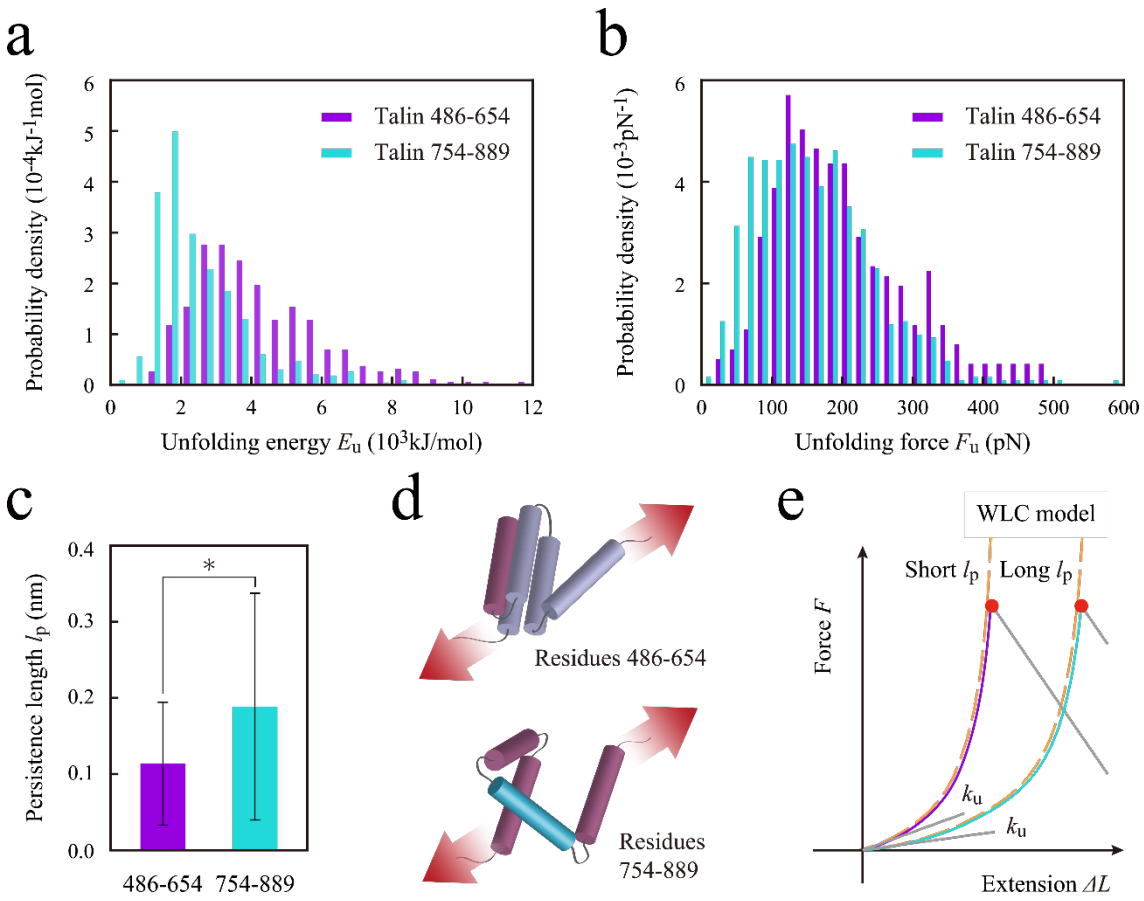

Fig. 3 Analysis of nano-mechanical behaviors.

(a) Unfolding energy E_u for the complete unfolding of talin. The histograms of

unfolding energy E_u for residues 486–654 (purple bars) and 754–889 (cyan bars). Residues 754–889 exhibited a right-skewed distribution with a lower mode value than that for residues 486–654. **(b)** Unfolding force F_u at force peaks. The histograms of unfolding force F_u for residues 486–654 (purple bars) and 754–889 (cyan bars). Residues 754–889 showed the distribution in low unfolding force F_u (< 100 pN). **(c)** Persistence length l_p of intermediate conformations under tension. The persistence lengths for residues 486–654 (purple bar) and 754–889 (cyan bar). The significance of the difference in the average was tested by *t*-test (*, $p < 0.001$). **(d)** Schematics of intermediate conformations of residues 486–654 (top panel) and 754–889 (bottom panel). **(e)** The mechanical behaviors of intermediate conformations with short and long persistence lengths l_p, as shown in purple and cyan curve, respectively.